Improvement of the vertical mixing in chemistry transport modeling based on a 1.5-order turbulence kinetic energy-based eddy diffusivity closure scheme

Lei Jiang, Bertrand Bessagnet, Frédérik Meleux, Florian Couvidat, Frédéric Tognet

Atmospheric Research 279 (2022) 106394

Contents lists available at ScienceDirect

Atmospheric Research

journal homepage: www.elsevier.com/locate/atmosres

Improvement of the vertical mixing in chemistry transport modeling based on a 1.5-order turbulence kinetic energy-based eddy diffusivity closure scheme

Lei Jiang [a,b,*], Bertrand Bessagnet [a,b,1], Frédérik Meleux [a], Florian Couvidat [a], Frédéric Tognet [a]

[a] INERIS, National Institute for Industrial Environment and Risks, Parc Technologique ALATA, 60550 Verneuil-en-Halatte, France
[b] Sorbonne University, UPMC Univ Paris 06, DE129, 75005 Paris, France

ARTICLE INFO

Keywords:
Air quality
Urban
Modeling
Vertical diffusion
High resolution

ABSTRACT

In this study, firstly, three first-order local closure vertical diffusion schemes used in multiple mesoscale chemical transport models (CTM) were embedded in the CHIMERE CTM model and tested over a one-year simulation covering the whole France. Three model configurations present a fair reproduction of pollutant concentrations both in urban and rural areas, indicating it is an effective way to reproduce the dispersion of pollutants in chemistry transport modeling. However, it cannot be expected to significantly improve the vertical mixing under the first-order closure scheme. Secondly, a 1.5-order turbulence kinetic energy-based eddy diffusivity closure scheme called as the new eddy diffusion (NED) is implemented in CHIMERE to describe more realistic diffusion processes near the surface. A fifteen-day simulation encompassing a winter pollution episode was performed for three major cities with horizontal resolution of 1.67 km and the first layer height at 12 m, respectively. The NED scheme improved NO_2 simulations at most urban sites compared to the initial *Kz* diffusion scheme (IKD). Taking the root mean square error as evaluation criteria, the average improvements are 18.8%, 24.5% and 9.5% for NO_2 simualtion in Paris, Lyon and Bordeaux respectively. For the model performance of $PM_{2.5}$ and PM_{10} simulations in the urban areas of Paris, the improvements are 13.5% and 19.1%, respectively. Overall, preliminary outcomes of this study are encouraging. The simulation with more sophisticated and realistic eddy viscosities are better than for IKD that is widely used in CTMs, but we need to realize that this is only a fifteen-day simulation for three cities, for further research, longer periods are needed with a greater variety of meteorological situations to prove the universality of the NED scheme.

1. Introduction

Air pollution is one of the biggest public health hazards worldwide responsible for over 6 million premature deaths every year (Forouzanfar et al., 2016; Lim et al., 2012; Valari et al., 2020). In cities, air quality is a major concern for citizens and city managers (Baklanov et al., 2007). With the development of high performance computers and a better knowledge of the meteorology and air pollution sources, meteorological and air quality modeling have been widely used in the last decades, particularly in urbanized and industrialized areas (Colette et al., 2011; Gašparac et al., 2020; Stohl et al., 2015). Today, High resolution mesoscale chemistry–transport models (CTM) such as Community Multiscale Air Quality Model (CMAQ), Comprehensive Air quality Model with extensions (CAMx) or CHIMERE have achieved sufficient accuracy to be considered for urban air quality predictions (Byun and Schere, 2006; Fillingham, 2019; Sokhi et al., 2018; Terrenoire et al., 2015). However, urban air pollution patterns are rather variable and spatially heterogeneous (Wolf et al., 2020), the heat and chemicals released by transportation, together with the huge amount of waste from the consumption of human activities, are the main sources of urban atmospheric pollution. The movement of pollutants includes transport, dispersion and deposition (Hirabayashi et al., 2012). Transport is the movement caused by mean wind flow. Dispersion is caused by local turbulence. Deposition processes, including precipitation, scavenging and settling, cause pollutants to move downward and will eventually settle to the surface (Amodio et al., 2014). Besides, geographical

* Corresponding author at: INERIS, National Institute for Industrial Environment and Risks, Parc Technologique ALATA, 60550 Verneuil-en-Halatte, France.
E-mail address: 200038@nuist.edu.cn (L. Jiang).
[1] Now at European Commission, Joint Research Centre (JRC), 21027 Ispra, Italy.

https://doi.org/10.1016/j.atmosres.2022.106394
Received 12 April 2022; Received in revised form 10 August 2022; Accepted 10 August 2022
Available online 16 August 2022

condition also plays an important role in transportation and dispersion of pollutants. Pollutants dispersion processes over the valley-basin city are much more complicated than over flat areas. Therefore, pollution episodes have been frequently witnessed over complex terrain, especially in wintertime (Chen et al., 2019; Sabatier et al., 2020).

There are various types of artificial surfaces in urban areas, such as asphalt roads, concrete sidewalks, glass curtain walls, parking lots, and green spaces which have impact on urban air quality (Wise, 2016). For example, computational fluid dynamics studies indicated that the flow resistance of tree crowns decreased wind speed and the dispersion of pollutants is limited in the ground level and the particulate matter concentrations accumulate within the canyon (Gromke and Blocken, 2015). These diversified types of artificial areas appear alternately, leading to complex, diverse, and non-uniform urban canopy characteristics, which give more complex turbulent airflows in urban region, increased the difficulty of air quality simulation and forecast in cities than in other regions. Thus, the interactions between urban and the atmosphere remains challenging (Letzel et al., 2008), especially to simulate airflows and dispersion within the urban canopy (Baker et al., 2004). Turbulence plays an important role on the vertical mixing of pollutants and other physical parameters (Menut et al., 2013a, 2013b; Pierce et al., 2010), but the representation of turbulence is difficult to predict particularly close to the ground levels. Studies have found that models tend to underestimate pollutant concentrations in urban areas when there is an explosive increase in pollutant concentrations, mainly due to inadequate turbulence treatment within the boundary layer (Huszar et al., 2020; Kurppa et al., 2018). All CTMs must account for the problem of turbulence, even if turbulent processes are still not fully understood (Argyropoulos and Markatos, 2015; Novati et al., 2021). For mesoscale CTM models, the turbulent diffusion is mainly based on the gradient transport theory (*K-theory*) which is a first order turbulence closure. It defines the turbulence fluxes as analogous to molecular transport, assuming that the turbulence is a fluid parcel, which has the same properties as the molecular transport model, and a linear relationship between the gradient and the flux is thus obtained (Huang, 2019; Klimontovich, 1985). This local turbulence closure approach assumes that turbulence consists of only small eddies, causing diffusion-like transport. For example, the vertical kinematic flux $\overline{w'c'}$ of a pollutant can be modeled as being equal to an eddy thermal diffusivity K times the vertical gradient of mean concentrations $\bar{c}$.

$$\overline{w'c'} = -\mathrm{K}\frac{\partial \bar{c}}{\partial z} \tag{1}$$

Also, the near-surface flow is complex process to simulate, the nature of turbulent transport is far from a simple linear relationship, it changes with the spatial scale of the atmospheric turbulence field and this notion of scale for turbulence is of major importance (He et al., 2019). In mesoscale model, the grid size is considerably larger than the energy containing turbulence scale, the turbulent energy is clearly in the unresolvable sub-scale (Wyngaard, 2004). Therefore, the turbulence can be parameterized instead of explicitly resolved. Currently, the most mainstream turbulence parameterization method is based on the first-order local closure scheme. Many studies show that this concise method is reliable under unstable and neutral conditions. However, the high pollutants concentrations are frequently observed under very stable conditions usually associated with cold weather (Wolf-Grosse et al., 2017; Zilitinkevich and Esau, 2005), which makes harder to provide an accurate prediction of pollution level and the early warning of pollution episode (PE). The traditional turbulence parameterization scheme is contaminated by submesoscale motions during PE, which makes the application of similar theory difficult and this is an important reason why models tend to underestimate pollutant concentrations during PE. A way to improve the turbulence parameterization is to increase the order of the closure (Stull, 1988).

The first part of this study addresses the results of the one-year air quality simulation that was determined by three first order *K-theory* vertical diffusion coefficient (*Kz*) from three mesoscale models (CHIMERE, CMAQ and FALL3D) respectively defined as *Kz1, Kz2* and *Kz3*. Inter-annual trends, seasonal and daily variations of main pollutants concentrations are presented. Here, it has been chosen to focus on both cities and surroundings in whole France domain. Then, in view of the shortcomings of the first order *K-theory* scheme, two new configurations based on the initial *Kz* in CHIMERE (*Kz1*) were applied in urban areas.

In the second part of the study, we use the eddy diffusion from the 1.5-order closure TKE embedded in the Weather Research and Forecasting (WRF) model as a new *Kz* in the CTM CHIMERE to describe more realistic diffusion processes near the surface for urban pollution applications. Two schemes are defined: one as the initial *K-theory* diffusion (IKD) scheme in CHIMERE and one as the new eddy diffusion (NED) scheme from WRF respectively. A high spatial resolution simulation, which is conducted for a winter period from 20th November to 4th December 2016 over three major cities (Paris, Lyon and Bordeaux) in France was performed with the WRF/CHIMERE suite. The results are presented in terms of model performances between the configurations for the usual criteria pollutants. The goal of this study is to propose a more advanced diffusion scheme to improve air quality simulations and forecast over urban and peri-urban area especially on the short-term pollution events.

2. Model description and experiment design

2.1. Experiment design for the first order K-theory study

The first step addresses the results of the one-year air quality simulation that was performed with three different first order local closure *K-theory* scheme to estimate the *Kz* within the boundary layer. The initial *Kz* in CHIMERE is defined as Eq. (2):

$$K_z = k w_s z\left(1-\frac{z}{h}\right)^2 \tag{2}$$

where k is the von Karman constant set to 0.41 in the model, z is the altitude, h is the boundary layer height, and w_s is the vertical scale given by the similarity formulae. Convective turbulence driven by buoyancy dominates during the day, while turbulence driven by wind shear at night is more dominant (Warner, 2010).

In stable conditions (h/L $\geq$ 0), the w_s is defined as (3):

$$w_s = \frac{u_*}{1+4.7z/L} \tag{3}$$

In unstable conditions (h/L $<$ 0), the w_s is defined as (4):

$$w_s = \left(u_*{}^3 + 2.8\alpha w_*{}^3\right)^{1/3} \tag{4}$$

where α = max (0.1, z/h), u_* is the fractional velocity, w_* is the convective velocity, L is the Monin–Obhukov length (Menut et al., 2013a). The Monin–Obukhov similarity theory widely used in mesoscale CTM model and it has many expressions. For the k-theory in the CMAQ, the *Kz* is defined by (Holtslag and Boville, 1993) as (5):

$$K_z = k\frac{u_*}{w_s} z\left(1-\frac{z}{h}\right)^2 \tag{5}$$

In stable conditions, the w_s is defined as (6):

$$w_s = 1+5\frac{z}{L} \tag{6}$$

In unstable conditions, the w_s is defined as (7):

$$w_s = \left(1-16\frac{z}{L}\right)^{-\frac{1}{4}} \tag{7}$$

In a three-dimensional Eulerian model (FALL3D)(Folch et al., 2009),

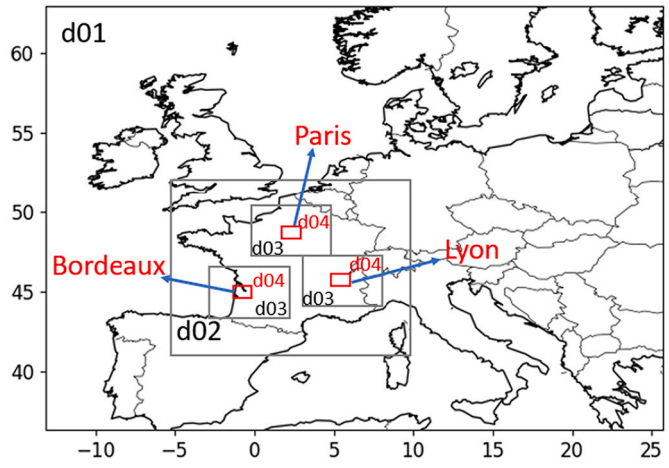

Fig. 1. Four nested domains—from the coarsest resolution d01, to the highest resolution d04.

Kz is defined as (Costa et al., 2006) (8):

$$K_z = ku_* w_s z\left(1-\frac{z}{h}\right) \tag{8}$$

In stable conditions, the w_s is defined as (9):

$$w_s = \left(1+9.2\frac{z}{L}\right)^{-1} \tag{9}$$

In unstable conditions, the w_s is defined as (10):

$$w_s = \left(1-13\frac{z}{L}\right)^{\frac{1}{2}} \tag{10}$$

An example of mass conservation is shown in Fig. S1 and more detail explanation of *Kz* can be found in Supporting Information Text S1.

As a first analysis, a long-term simulation covering the entire year 2016 has been performed with three *Kz* parameterizations as previously mentioned. The *Kz* from CHIMERE, CMAQ and FALL3D are defined as *Kz1, Kz2* and *Kz3* respectively. Among them, the *Kz1* scheme is the initial vertical diffusion scheme of the CHIMERE model. We tested several schemes based on first order *K-theory* vertical diffusion and finally selected *Kz2* and *Kz3* as the reference schemes for this study. A minimal *Kz* is setup to $0.01 m^2/s$ in the dry boundary layer and $1 m^2/s$ in the cloudy boundary layer in three schemes to avoid unreasonable low mixing (Menut et al., 2013a, 2013b).

The simulation is performed from 1st January to 31st December 2016 at 7 km horizontal resolution over France which maintain a consistent horizontal resolution for the French air quality monitoring platform PREV'AIR. The domain is discretized vertically with 20 vertical levels from 998.5 hPa to 500 hPa, with the lowest level at about 12 m and 14 levels below 1000 m. Meteorological input data were taken from the Integrated Forecasting System (IFS) model from the European Centre for Medium-Range Weather Forecasts (ECMWF) available at a 7 km resolution at six-hourly time steps. Chemical boundary conditions were obtained from a lower (25 km) resolution simulation performed on a European domain. The sector specific European Monitoring and Evaluation Program (EMEP) inventory (details can be found in https://www.emep.int/) and French National Spatialized Emission (INS) Inventory has been used for anthropogenic emissions in the model, at a resolution of 0.1°x 0.1°.

The air quality monitoring data are taken from the French Central Air Quality Monitoring Laboratory (LCSQA)(Honore et al., 2006). A total of 57 urban and 15 rural background air quality monitoring stations are selected. They provide hourly surface concentrations of criteria pollutants (NO_2, $PM_{2.5}$, and PM_{10}) and are used to assess the performances of the models with the various *Kz* parameterizations, the locations of stations is shown in Supporting Information Fig. S2.

To quantify the difference between model and instruments data, mean bias (MB), mean linear correlation coefficient (R) and root mean square error (RMSE) is used to assess the performances. The definition of RB, MB, R and RMSE is shown in the Text S2.

2.2. Model description and observations data for the second study

On the second step of this experiment the WRF model (Version 3.9.1) provides the high resolution meteorological input data for the CTM. The simulation is performed from 20th November to 4th December 2016, including a three days heavy PE from 30th November to 2nd December. The initial and boundary conditions of WRF are issued from the Global Forecasting System (GFS) analysis data from the National Centers for Environmental Prediction (NCEP), available at a 0.25° × 0.25° resolution at six-hourly time steps. Anthropogenic emissions are generated with the EMEP and INS emission inventory, this is in line with the first part of the study. In order to calculate realistic meteorological input variables and pollutant concentrations, the system is configured with four nested-grid domains over three areas Paris, Lyon and Bordeaux (as shown in Fig. 1) with 106 × 91, 118 × 115, 115 × 103 and 85 × 79 grid points, with cell sizes of 45 km (d01), 15 km (d02), 5 km (d03), and 1.67 km (d04) horizontal resolution, respectively. The domain size and resolution are the same for the three areas. The model physical parameters setting are based on our previously study (Jiang et al., 2020).

The CTM model CHIMERE (Version 2013) (Menut et al., 2013a, 2013b) is used for air quality modeling in the present study. CHIMERE is a state-of-the-art Eulerian offline CTM model using a mass conservative approach to reproduce pollutant chemical transformations and transport. The initial vertical diffusion of CHIMERE called as IKD in this study is based on first order closure scheme, it is mostly controlled by the PBL height. The horizontal diffusion is is set as a constant value ($1 m^2/s$) in CHIMERE. The PBL height is directly read from WRF and capped at a minimal value of 20 m to avoid unrealistic simulations. In CHIMERE, the *Kz* is calculated as Eq. (2).

Many studies indicate this first order closure *K-theory* is appropriate for mesoscale modeling particularly for neutral to weakly stable conditions. However, our previous studies (Jiang et al., 2020) found that the difference in simulated $PM_{2.5}$ concentrations during heavy pollution episode could be as high as two to five times according to different planetary boundary layer (PBL) schemes. Some of the PBL schemes cannot effectively simulate the height of the boundary layer during the pollution period, resulting in the simulated pollutants concentrations several times higher than the observations. There are generally two ways to improve the mesoscale vertical mixing. The first is to use a higher-order local closure scheme to replace the turbulence parameterization scheme. Second, use non-local closure scheme, the unknown quantity on the grid point can be determined by the known quantity on the grid point farther away in the vertical direction rather than only determined by the same grid (Warner, 2010).

The WRF Version 3.9.1 provides 13 PBL schemes that can be classified mainly according to critical Richardson number or TKE, commonly referred to as first-order closure and TKE closure schemes for PBL turbulence modeling and PBL height determination(Tyagi et al., 2018). The TKE order-1.5 model was calculated from Boulac PBL scheme defined as NED scheme in the second step of this study. The computation strategy of NED can be separated into the following sequential steps:

i. Activate the *Kz* output (variable "vertical eddy viscosity" in the WRF Registry), because it is not a default output variable in WRF;
ii. Perfom WRF simulation based on Boulac PBL scheme and store calculated *Kz* values (NED);
iii. Pre-processing in CHIMERE: Interpolate NED to CHIMERE;
iv. Initialization phase of CHIMERE simulation, replacing IKD with NED;

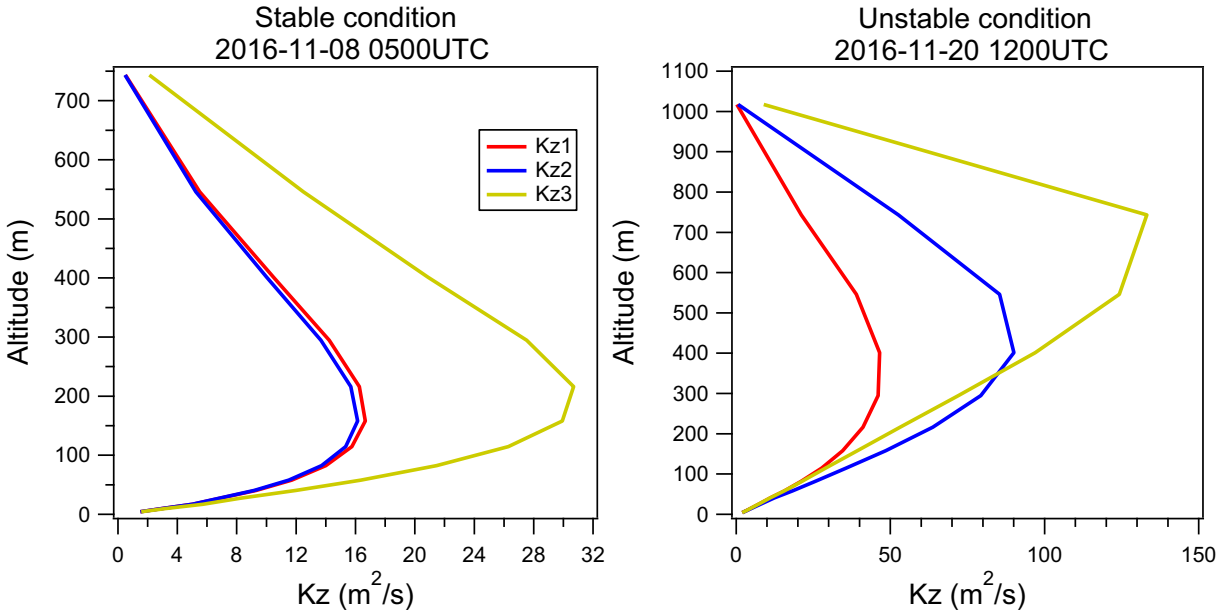

Fig. 2. Sensitivity test of vertical profile of Kz (m^2/s) in stable and unstable conditions.

v. Launch the main step of CHIMERE simulation and get all output variables based on NED.

The prognostic equation for TKE e under the assumptions of horizontal homogeneity can be written as (11):

$$\frac{\partial e}{\partial t} = -\frac{\partial}{\partial z}\left(\overline{w'e} + \frac{\overline{w'p'}}{\rho_0}\right) + \frac{g}{\theta_{v0}}\overline{w'\theta_v} - \left(\overline{w'u'}\frac{\partial v}{\partial z} + \overline{w'v'}\frac{\partial u}{\partial z}\right) - \varepsilon \tag{11}$$

Where u, v, w are the wind components, θ_v is the mean virtual potential temperature, p is the pressure, $\rho_0$is the density, g is the gravitational acceleration and ε is the viscous dissipation of TKE (Stull, 1988).

The 1.5-order TKE is also constructed based on gradient transport theory as (12):

$$\overline{w\phi} = -K\frac{\partial \phi}{\partial z} \tag{12}$$

The left side represents the Reynolds-average operator, the vertical turbulent flux $\overline{w\phi}$ is parameterized as the product of local gradient of analytical variable ϕ and eddy diffusivity K. In Boulac scheme, vertical eddy diffusivity is defined as (13):

$$K_z = C_k l\sqrt{e} \tag{13}$$

Where C_k is a constant set up to 0.7, l is the vertical length scale (Deardorff, 1980), and e is the TKE defined as (14):

$$e = \frac{1}{2}\left(\overline{u'^2} + \overline{v'^2} + \overline{w'^2}\right) \tag{14}$$

In Boulac scheme, it is assumed that at individual level in the atmosphere, the length scale l may be related to the distance that the parcel originating from the corresponding level and having the initial kinetic energy equal to the average TKE of the layer which can move up and down before being prevented by the buoyancy effect (Bougeault and Lacarrere, 1989). The l_{up} and l_{down} is defined as (15):

$$\begin{aligned}\int_{Z}^{Z+l_{up}} \beta(\theta(Z) - \theta(Z'))dZ' &= e(Z)\\ \int_{Z+l_{down}}^{Z} \beta(\theta(Z) - \theta(Z'))dZ' &= e(Z)\end{aligned} \tag{15}$$

Thus, the length scale l will assume a value between l_{up} and l_{down}. In Boulac scheme, the l is written as (16):

$$l = \sqrt{(l_{up}l_{down})} \tag{16}$$

The advantage of this scheme is to allow for remote effects of stable zones to define the turbulence mixing length scale (Bougeault and Lacarrere, 1989). This vertical mixing scheme solves a prognostic TKE equation which includes TKE advection and parameterizes sources and sinks from shear production, buoyancy, mixing and dissipation (Simon et al., 2019). Here we need to emphasize that the TKE calculation is a one-way method, and therefore does not affect the performance of there corresponding boundary layer scheme.

The hourly surface concentrations of criteria pollutants (NO_2, $PM_{2.5}$, and PM_{10}) issued from LCSQA. The location of the air quality monitoring stations (AQS) can be found in Fig. S3.

3. Results and discussions

3.1. The first order K-theory tests

3.1.1. Vertical distributions of the first order K-theory tests

A sensitivity test using the same model configurations, but different vertical diffusion coefficients was performed to understand the role of each *Kz* in stable and unstable conditions. As shown in Fig. 2, three schemes display similar *Kz* at low levels in stable condition, with a relatively high surface diffusion rate in *Kz3* and relatively low surface diffusion rate in *Kz2*, the *Kz1* shows a slightly higher *Kz* in all levels. However, *Kz3* has obviously stronger *Kz* in middle levels. Under unstable conditions, the ground level *Kz* shows a completely opposite trend to stable condition, with *Kz2* > *Kz1* > *Kz3* at ground level. In the middle levels, the difference between the different schemes is significantly higher than the stable condition. The yearly averaged vertical profiles of *Kz*, NO_2, O_3, $PM_{2.5}$ and PM_{10} can be found in Fig. S4, and the seasonal variations of main pollutants can be found in Fig. S5. Models underestimated NO_2 concentrations whatever the season, but particularly during wintertime. The negative biases are −6.1 μg/m^3, −6.2 μg/m^3 and − 7.1 μg/m^3 for *Kz1*, *Kz2* and *Kz3* in winter respectively, it can indicate the model may overestimate vertical mixing in urban region. The model displays relatively better performances in $PM_{2.5}$ simulation, with slight negative biases in summer and positive biases in the rest of seasons. However, three schemes underestimated PM_{10} concentrations in every season. The ratio of $PM_{2.5}$ /PM_{10} exceeds 90% in all seasons in

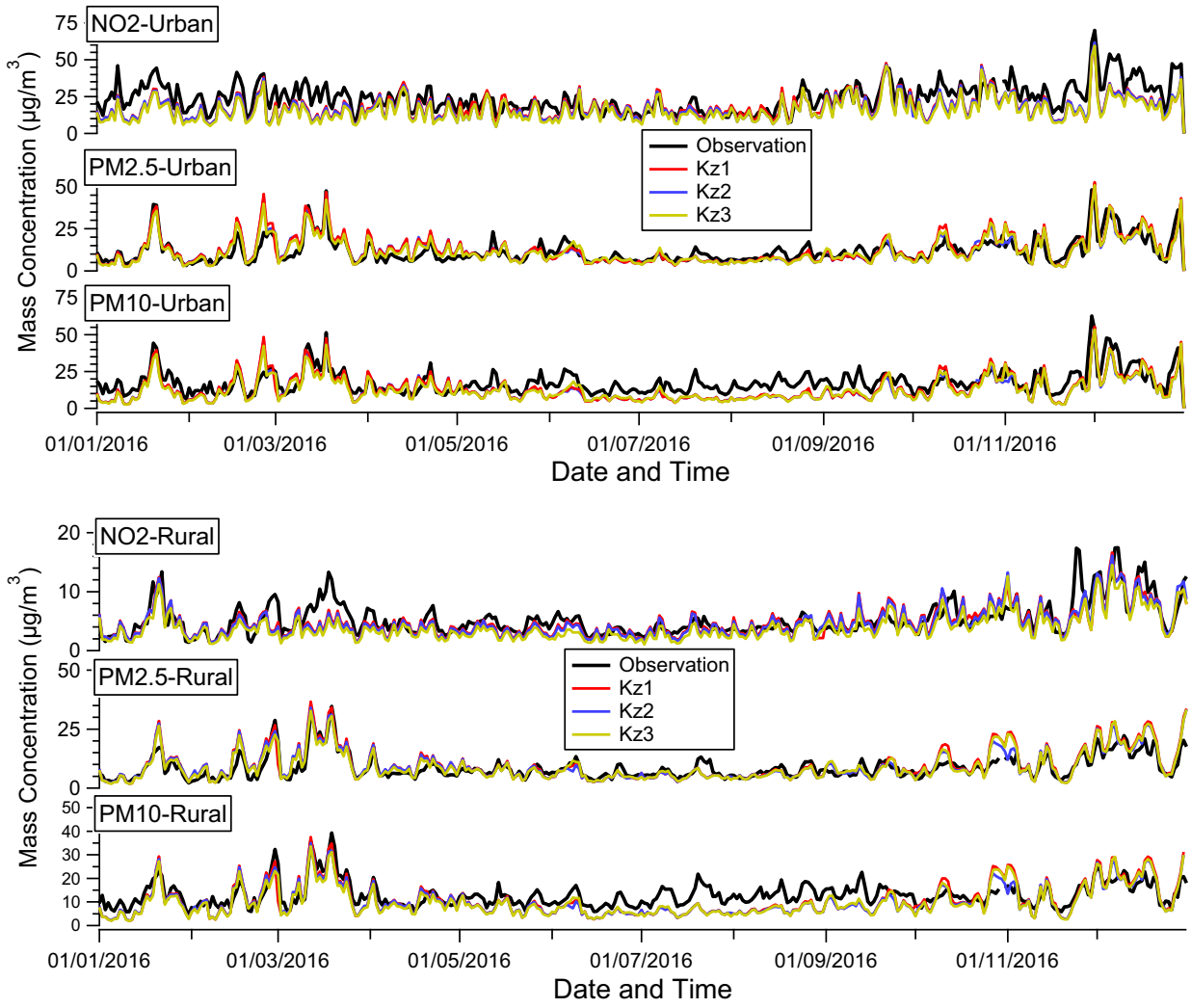

Fig. 3. Time series between observed and modeled NO_2, $PM_{2.5}$ and PM_{10} mass concentrations (μg/m^3) in Urban and Rural areas over the whole France domain.

the tests, while the ratio is usually around 70% in the observations. This could also indicate the underestimation of coarse particles in the emission inventory, natural or anthropogenic in origin.

3.1.2. *Comparison of model results with observations*

In order to better evaluate the impact of vertical diffusion coefficients on the air quality predictions, modeled time series of the pollutants concentrations compared with the observations for urban and rural region are displayed in Fig. 3. In urban areas, the models capture the time variability quite well for NO_2, $PM_{2.5}$ and PM_{10} simulations, particularly for the $PM_{2.5}$, model well reproduced the seasonal variability. However, the model tends to underestimate the NO_2 and PM_{10} concentrations in urban areas especially during wintertime for NO_2 and summertime for PM_{10}. The yearly average surface mass concentrations of $PM_{2.5}$ and PM_{10} are respectively 10.4 μg/m^3 and 15.4 μg/m^3 from the observation over the France domain, the ratios of $PM_{2.5}/PM_{10}$ 67.3% in the observation. In the cases of simulations, $PM_{2.5}$ surface concentrations are 10.8 μg/m^3, 11.2 μg/m^3, 10.6 μg/m^3 and PM_{10} surface concentrations are 11.7 μg/m^3, 12.1 μg/m^3, 11.5 μg/m^3 from *Kz1, Kz2* and *Kz3*, respectively. The ratios of $PM_{2.5}/PM_{10}$ are almost the same which is approximately 92.5% for three schemes, the bias of the ratios of $PM_{2.5}/PM_{10}$ is approximately 25.3% compare to observations. The diurnal cycle of main pollutants is shown in the Fig. S6. The diurnal cycles of NO_2, $PM_{2.5}$ and PM_{10} have a similar behavior at urban sites, with two

Table 1
Statistics of surface variables: mean linear correlation coefficient (R); mean bias (MB) and root mean square error (RMSE) between the simulations and observations of NO_2, $PM_{2.5}$ and PM_{10} in Urban and Rural areas.

		NO_2			$PM_{2.5}$			PM_{10}		
		Kz1	Kz2	Kz3	Kz1	Kz2	Kz3	Kz1	Kz2	Kz3
Urban	R	0.73	0.76	0.74	0.83	0.83	0.84	0.74	0.75	0.76
	MB	−6.4	−7.1	−8.4	0.56	0.16	−0.10	−4.3	−4.7	−5.0
	RMSE	9.3	9.6	10.6	4.8	4.5	4.3	7.4	7.6	7.5
Rural	R	0.72	0.73	0.73	0.88	0.88	0.87	0.78	0.77	0.77
	MB	−0.47	−0.62	−1.3	1.1	0.67	0.56	−2.4	−2.8	−2.9
	RMSE	2.1	2.1	2.4	3.7	3.3	3.3	5.2	5.1	5.2

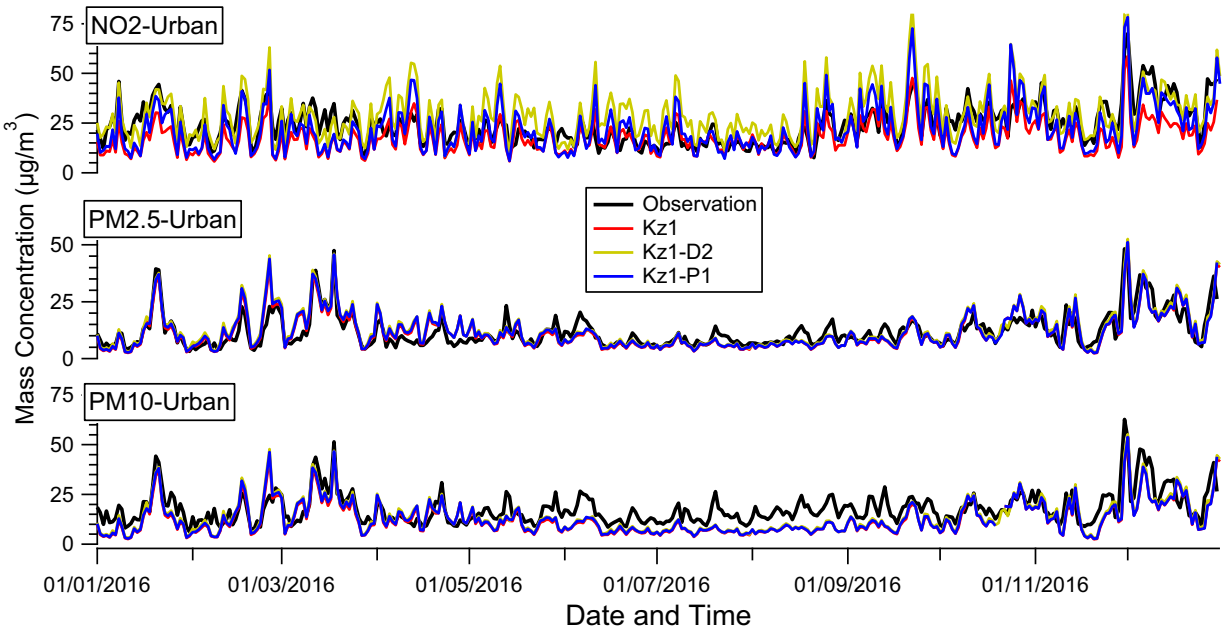

Fig. 4. Time series between observed and modeled NO_2, $PM_{2.5}$ and PM_{10} mass concentrations (μg/m^3) in Urban areas over the whole France domain.

peaks occurred in the morning and evening rush hours. In rural areas, the evening peak did not appear, with a gradual accumulation at nighttime. Compared with observations, the simulations display more significant diurnal differences for all pollutants, and the model significantly underestimates the concentration of NO_2 and PM_{10} during daytime. This indicates that the *K-theory* schemes may overestimate the vertical mixing under unstable conditions. All three schemes in rural areas display a quite good reproduction of the evolution of pollutant concentrations and better capture the fluctuations of pollutants in the wintertime and for urban areas. The models underestimate PM_{10} concentrations particularly in summertime. Table 1 provides an overall evaluation of the three schemes in urban and rural areas including R, MB and RMSE. In general, the models present a better performance in rural than urban areas. NO_2 and PM_{10} concentrations are largely

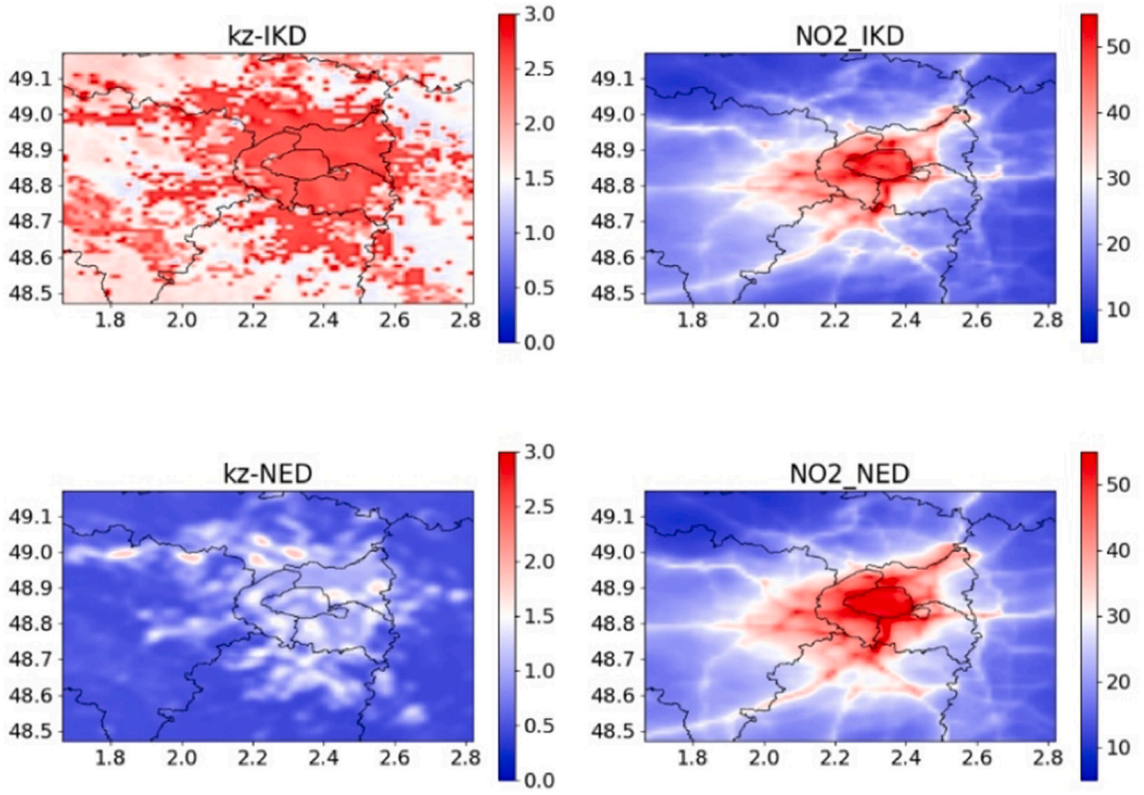

Fig. 5. Maps of the mean vertical diffusion coefficient (m^2/s) at first layer (12 m); mean surface NO_2 mass concentration (μg/m^3) over the period from 20th November to 4th December. The first line: results from IKD scheme; the second line: results from NED scheme.

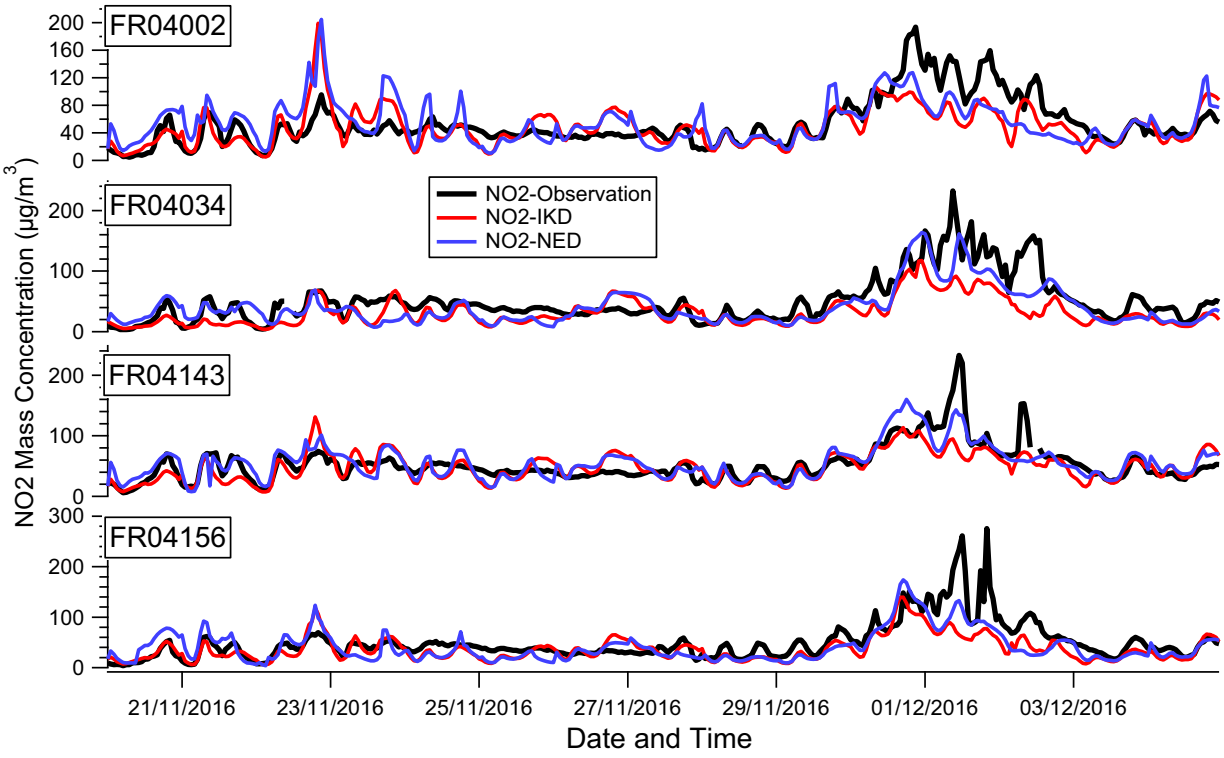

Fig. 6. Time series between observed and modeled NO_2 mass concentration (μg/m^3) at urban background stations.

underestimated in urban areas than for rural areas. This indicates the model overestimates vertical mixing in urban areas to some extent by comparing it to rural areas, although vertical mixing is only one of the causes of error. The value of exponent p is considered as 2 (the "square" in the equation) in Eqs. (1) and (5). The range of this value has been considered from 1 to 3 by Troen and Mahrt (Troen and Mahrt, 1986), the vertical mixing varies considerably correspond to the range of p from 1 to 3 (Hu et al., 2010). Therefore, the results show that setting p value to 2 is applicable in rural areas, but the p value is overestimated in urban areas. An easy way to improve such a first order local closure scheme is to set p according to types of land use. Comparing the performances of three *k-theory* schemes and taking RMSE as the criterion for judging the ability of the model, as shown in Table 1 the differences between the test results are small. Therefore, it cannot be expected to significantly improve the mesoscale model for air quality simulation and forecast through the modification of diffusion coefficient based on first order local closure scheme.

3.1.3. Additional tests based on Kz diffusion in CHIMERE

Previous studies demonstrate all three schemes underestimates NO_2 concentrations in cities therefore three schemes may overestimate vertical mixing in urban areas because NO_2 is typically a "local" pollutant. In this section, two new tests based on the *Kz1* as Eq. (2) is applied as the new *Kz* in urban areas over France.

In the first test, we divide the *Kz1* by 2 in urban region, the new *Kz* called as *Kz1-D2* and defined as in Eq. (16):

$$K_z = 0.5 * k w_s z \left(1 - \frac{z}{h}\right)^2 \tag{16}$$

In the second test, we decrease the p value from 2 to 1 in the *Kz1* in urban region, the new *Kz* called as *Kz1-P1* and defined as in Eq. (17):

$$K_z = k w_s z \left(1 - \frac{z}{h}\right) \tag{17}$$

The time evolution of hourly-averaged NO_2, $PM_{2.5}$ and PM_{10} between observation and three tests involved in the inter-comparison is provided in Fig. 4. In general, the two new tests simulated higher surface NO_2 concentrations in urban areas compared with the *Kz1*. The average NO_2 concentrations are 17.9 μg/m^3, 29.2 μg/m^3, 22.2 μg/m^3 from *Kz1*, *Kz1-D2* and *Kz1-P1*, respectively. The small differences between the tests can be found in $PM_{2.5}$ and PM_{10} simulations. This result is acceptable, because NO_2 mainly comes from local emissions which is more sensitive to the vertical diffusion rate and PM is affected by both local emissions and regional transport. As shown in Table S1, *Kz1-P1* gives a slightly better performance for all pollutants. The agreement with observations is generally better than for the other two cases. The *Kz1-D2* test overestimated NO_2 surface concentrations, which indicates that dividing the vertical diffusion rate by two could underestimate vertical mixing in urban region. The results again demonstrate that through the modification of vertical diffusion coefficient based on first order local closure scheme cannot significantly improve the ability of the CTM.

3.2. Model performance based on initial Kz and new eddy diffusion

3.2.1. NO_2 simulation in urban background stations of Paris

The surface temperature varies between −1.4 °C and 9.3 °C during this time period, with an average of 4.0 °C at urban region of Paris, the average surface wind speed was 2.3 m/s, no rainfall during this period.

Road traffic emission is the largest contribution to NO_2 concentrations in urban areas (Dragomir et al., 2015; Lee et al., 2014; Palmgren et al., 1996). The mean first layer NO_2 concentrations and *Kz* over the period are shown in Fig. 5. The results show that the absolute values are different between the IKD and NED schemes, the regional patterns are similar for the *Kz* and the two pollutants. It is a bit obvious that the results over urban areas exhibit the role of NO_x emissions on NO_2 concentrations. The *Kz* simulated by the NED method is significantly lower than the IKD scheme over the entire region. The average surface *Kz* from NED scheme is 1.1m^2/s in the urban region which is less than half of the IKD scheme (2.5m^2/s). Consequently, the NED scheme runs generate remarkably higher surface NO_2 concentrations by 6.9 μg/m^3 on average in urban area.

Table 2
Average modeled NO_2 mass concentrations (Avg); the correlation (R); mean bias (MB) and root mean square error (RMSE) between Observation and simulation of NO_2 in four urban background stations over Paris region.

	IKD				NED				
	Avg	R	MB	RMSE	Avg	R	MB	RMSE	improvement[a]
FR04002	48.3	0.62	−5.11	28.1	54.4	0.57	0.94	30.3	−7.8%
FR04034	31.1	0.74	−18.93	32.1	40.0	0.78	−10.01	25.9	19.2%
FR04143	47.9	0.67	−4.49	23.7	55.4	0.78	2.91	20.2	14.7%
FR04156	36.8	0.69	−12.87	30.7	40.8	0.72	−8.85	28.2	8.0%

[a] The "improvement" is the relative change in % of the RMSE by using the initial Kz diffusion (IKD) coefficient and by using the new eddy diffusion (NED) coefficient.

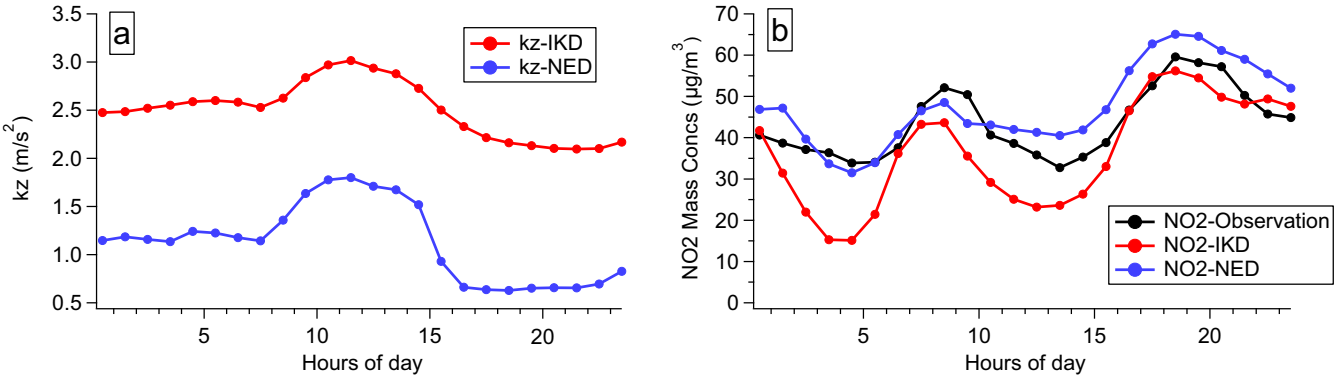

Fig. 7. Diurnal cycles for surface Kz and surface concentrations of NO_2 (μg/m^3) from 20th November to 4th December in urban background stations.

Fig. 6 shows the time series of hourly averaged mass NO_2 concentrations, from all urban background stations from November 20th to December 4th 2016. The linear regression of NO_2 between observations and simulations can be found in Fig. S7. Compared to the IKD scheme, the NED scheme showed better correlation with observations for all sites. Relatively high NO_2 concentrations were observed in all four urban background stations, with a mean concentration of 53.5 μg/m^3; 50.1 μg/m^3; 52.5 μg/m^3; 49.7 μg/m^3 in FR04002; FR04034; FR04143; FR04156 station, respectively. Table 2 lists the performances of NO_2 simulation for both schemes with their average mass concentration (Avg); R; MB and RMSE at each station. The results show that the period is well modeled by the IKD scheme with a correlation from 0.62 to 0.74. However, this scheme seems to underestimate NO_2 concentrations at all stations, this is mainly because of the underestimation during the pollution episode (PE). The performance of NED scheme is very satisfactory and improves NO_2 simulations for most of stations.

Taking the relative change in % of the RMSE as the evaluation criteria of the model performances which defined as (18):

$$Imp(\%) = \frac{RMSE_{tes} - RMSE_{ref}}{RMSE_{ref}} * 100 \quad (18)$$

Where $RMSE_{tes}$ refers to the RMSE of the test case and $RMSE_{ref}$ refers to the RMSE of the reference case. The largest improvements occur for the south-Paris FR04034 station (improved by about 19.2%). The averaged time series and statistics for the urban background stations are summarized in Fig. S8 and Table S2. The two schemes capture quite well the evolution of NO_2 concentrations over the urban region, the R and MB are 0.74 and − 10.4 μg/m^3 for IKD scheme and 0.80 and − 3.8 μg/m^3 for NED scheme with the improvement is of 18.8% in the urban area. Fig. 6 also shows the ability of the model to locate the pattern of the PE but also a clear underestimation of NO_2 concentrations during the PE for all stations. At most of the sites, the peak concentration of NO_2 occurred during the daytime on December 1st, the NO_2 exceeded 200 μg/m^3 in the observations but the model did not effectively capture this time with both schemes. The average mean bias in urban background stations for IKD and NED schemes during the PE are −39.9 μg/m^3 and − 24.1 μg/m^3 respectively, showing a better ability of the NED simulation to reproduce primary pollutant concentrations.

3.2.2. *Diurnal cycles of the surface Kz, NO_2 in Paris region*

In order to investigate in-depth the differences between the schemes, the diurnal cycles are calculated for *Kz* and NO_2 and compared with the corresponding surface observations at the urban background stations over the Paris region. Fig. 7(a) illustrates the mean diurnal *Kz* on urban regions. The diurnal variation of the surface *Kz* throughout the schemes shows similar patterns, *Kz* remains flat in the morning and nighttime and a peak is simulated around 12:00. The average *Kz* on the unstable condition from IKD scheme is approximately 1.6 times than NED scheme and approximately three times higher than for the stable condition. The bimodal distribution of the surface NO_2 concentration are observed and simulated during this period, with the morning peak around 8:00–9:00 and the evening peak around 18:00–19:00. Both schemes capture the fluctuations quite well, but the IKD scheme strongly underestimates NO_2 concentrations in the early morning. The results of the first part study prove that the IKD scheme overestimates the vertical diffusion rate in urban areas. This section further demonstrates that overestimation of vertical diffusion under stable conditions is higher than under unstable conditions in IKD. The NED scheme simulation overestimates NO_2 concentration at nighttime, the reason should be the overestimation of *Kz* drop after 14:00.

3.2.3. *$PM_{2.5}$ and PM_{10} simulations in Paris region*

The maps of $PM_{2.5}$ and PM_{10} surface concentrations for IKD and NED schemes are illustrated in Fig. S9. The NED scheme showed better correlation with observations for all urban sites compared to the IKD scheme. The surface concentration fields show a gradient between the surroundings urbanized area in both schemes but not as strong as for NO_2 surface distributions, this result is expected because $PM_{2.5}$ and PM_{10} is much more influenced by regional transport and particularly by peri-urban and rural emissions from biomass burning. The $PM_{2.5}$ and PM_{10} surface concentrations from NED scheme is approximately 4.4 μg/m^3 and 4.2 μg/m^3 higher on average than for the IKD scheme.

Fig. 8 displays a comparison between the observed and modeled surface $PM_{2.5}$ and PM_{10} at urban sites. The direct comparison shows a

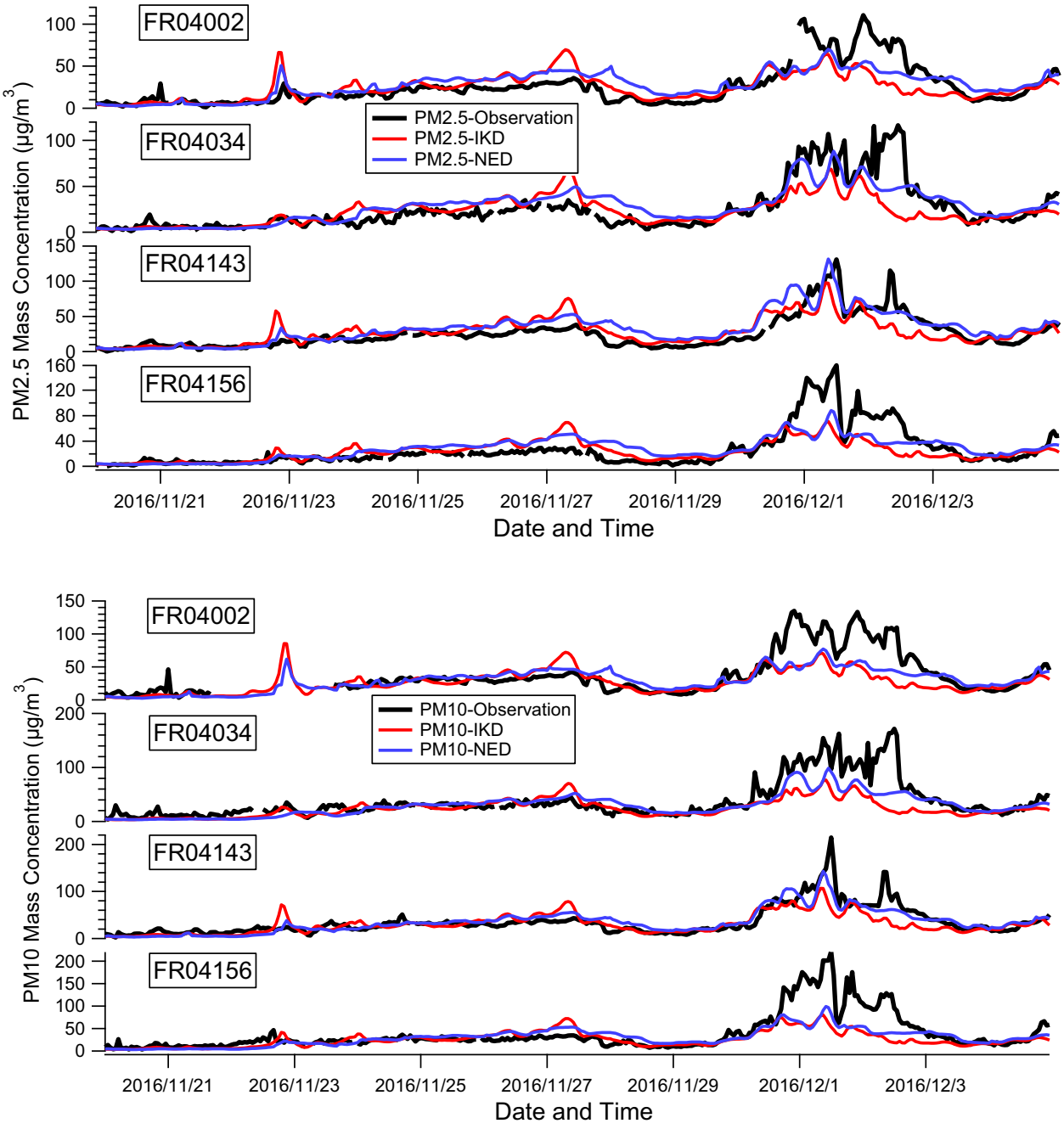

Fig. 8. Time series between observed and modeled $PM_{2.5}$ and PM_{10} mass (µg/m^3) in urban background stations.

Table 3
Average modeled $PM_{2.5}$ and PM_{10} mass concentrations (Avg); the correlation (R); mean bias (MB) and root mean square error (RMSE) between Observation and simulation of $PM_{2.5}$ and PM_{10} in urban background stations over Paris regions.

		IKD				NED				
		Avg	R	MB	RMSE	Avg	R	MB	RMSE	improvement
$PM_{2.5}$	FR04002	24.2	0.63	−1.4	18.2	27.7	0.74	2.2	16.2	11.0%
	FR04034	22.2	0.62	−3.3	20.3	27.3	0.81	1.8	15.6	23.1%
	FR04143	27.9	0.72	2.4	16.3	32.7	0.86	7.1	14.4	11.6%
	FR04156	23.5	0.66	−2.8	22.7	27.4	0.74	1.1	20.9	8.2%
PM_{10}	FR04002	26.6	0.66	−10.9	25.8	29.7	0.76	−7.8	22.1	14.3%
	FR04034	24.2	0.62	−13.4	30.4	29.3	0.80	−8.3	23.4	22.8%
	FR04143	30.3	0.70	−4.5	21.4	34.9	0.86	0.07	15.2	28.9%
	FR04156	25.7	0.70	−12.2	33.6	29.4	0.77	−8.5	30.1	10.3%

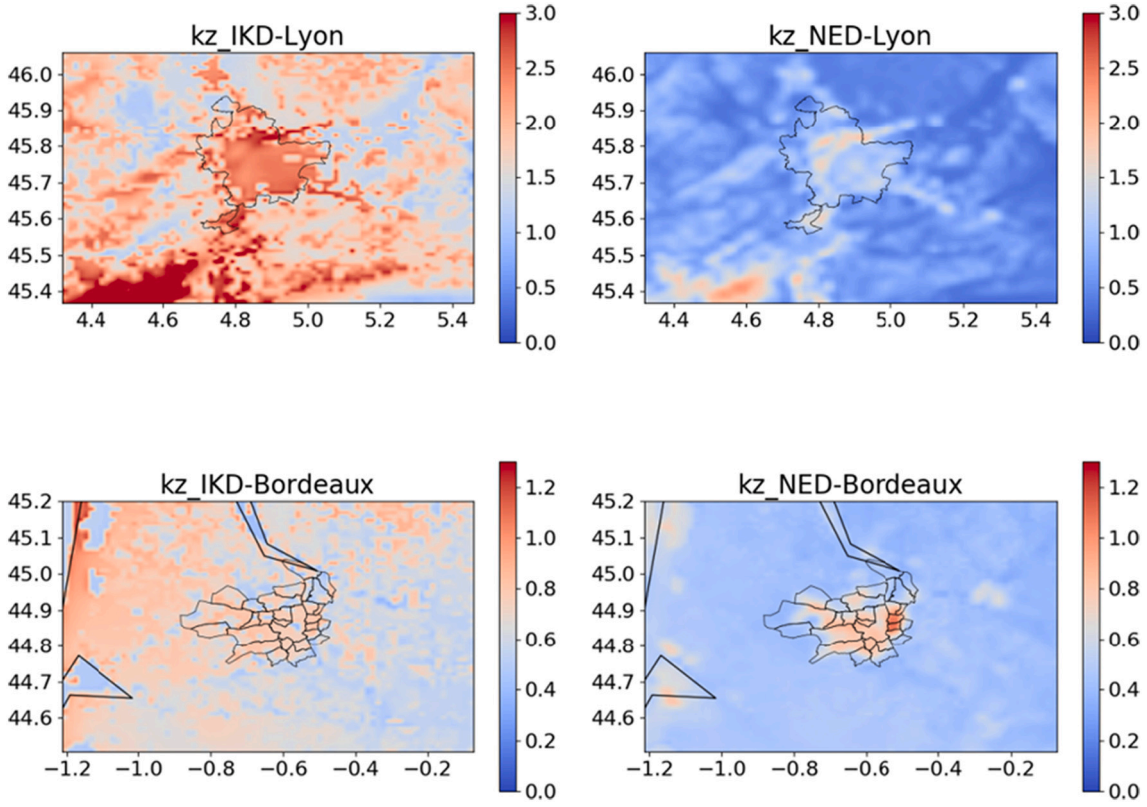

Fig. 9. Maps of the mean vertical diffusion coefficient (m^2/s); over the period from 20th November to 4th December. The first line: results from Lyon domain; the second line: results from Bordeaux domain.

fair reproduction of $PM_{2.5}$ and PM_{10} concentrations during the regular day but the models underestimate the concentrations on the PE. The fluctuations of $PM_{2.5}$ and PM_{10} at Paris center station (FR04143) is obviously different with others which indicate that the PM emissions at the center of the city is different with other sites, traffic emissions should be the major source of the FR04143 station. This also can be confirmed throughout the comparison between the fluctuations of NO_2 and PM in the corresponding station. Both schemes display similar behavior for the simulated period and display a reasonable representation of $PM_{2.5}$ and PM_{10} observations. The simulation of PM_{10} is good on regular day but the model tends to slightly overestimate $PM_{2.5}$ concentrations at the same time. It indicates the slight overestimation of fine particles in the model. Two schemes underestimated PM concentration during the PE, the NED scheme gives a higher $PM_{2.5}$ and PM_{10} concentrations than IKD scheme, which tends to be closer to the observations on the PE and the peaks of $PM_{2.5}$ and PM_{10} are also enhanced from NED. As shows in Table 3, the striking result is the NED scheme which improves the $PM_{2.5}$ and PM_{10} simulation at urban sites. Based on RMSE indicator, the improvements are almost >10% in every urban background station and the correlation are also significantly improved in the urban sites.

We also notice that the underestimation of PM_{10} is obviously higher than for $PM_{2.5}$ during the PE. There is no evident variation of this ratio on the PE for both observation and simulations, but the ratio is approximately 70% for the observation and around 90% for both simulations. Considering the overestimation of fine particles concentrations, this result shows that model have a strong underestimation of PM with particles exceeding 2.5 μm. The model displays a reasonable behavior for both $PM_{2.5}$ and PM_{10} on the PE, this indicates that the underestimation of pollutants on the PE is due to the underestimation of local urban pollution sources, vehicle emission and other local sources should play important roles on this period.

3.2.4. *NO_2 simulations in urban area over Lyon and Bordeaux regions*

The IKD and NED schemes are also applied in Bordeaux and Lyon areas in order to understand whether the NED scheme can be used in other areas. Lyon is in the southeast of France and is located in the Rhone valley where the wind is meridional and often strong particularly in winter and is the second largest city in France. Bordeaux is close to the sea that is often influenced by oceanic flows and located in the southwest part of France. The period of interest remains the same from 20th November to 4th December.

The mean first layer *Kz* for Lyon and Bordeaux domains over the period are displayed in Fig. 9 and surface NO_2 mass concentrations can be found in Fig. S10. Both domains present similar regional distribution when compared to the Paris domain. The NO_2 concentration are higher within the urban area and becomes patchier in the suburban and rural areas, these concentrations are higher near traffic sites.

The time series of the model predictions of the NO_2 mass concentrations compared to the observations for all urban background stations over Lyon and Bordeaux region are shown in Fig. 10. The linear regression between observed and modeled NO_2 can be found in Fig. S11. In general, the increase in NO_2 mass concentrations during PE in Lyon and Bordeaux region are not as pronounced as the case in Paris. This demonstrates that the PE in Lyon and Bordeaux were not primarily caused by local sources. In Lyon, it seems that there are two slight NO_2 pollution episodes during this period. One from 22nd November to 26th November and another from 30th November to 3rd December. Overall, both schemes capture the majority of fluctuations quite well in both regions. In particular, the NED scheme almost perfectly captures the first peak of NO_2, the 22nd December. However, although the IKD scheme captures the fluctuations of NO_2, NO_2 concentration are underestimated with IKD for the second light peak in Lyon from the nighttime of 30th November displayed in the observations.

Table 4 reports a detailed evaluation of NO_2 simulation for both schemes at each urban background station. As in Paris, the IKD scheme

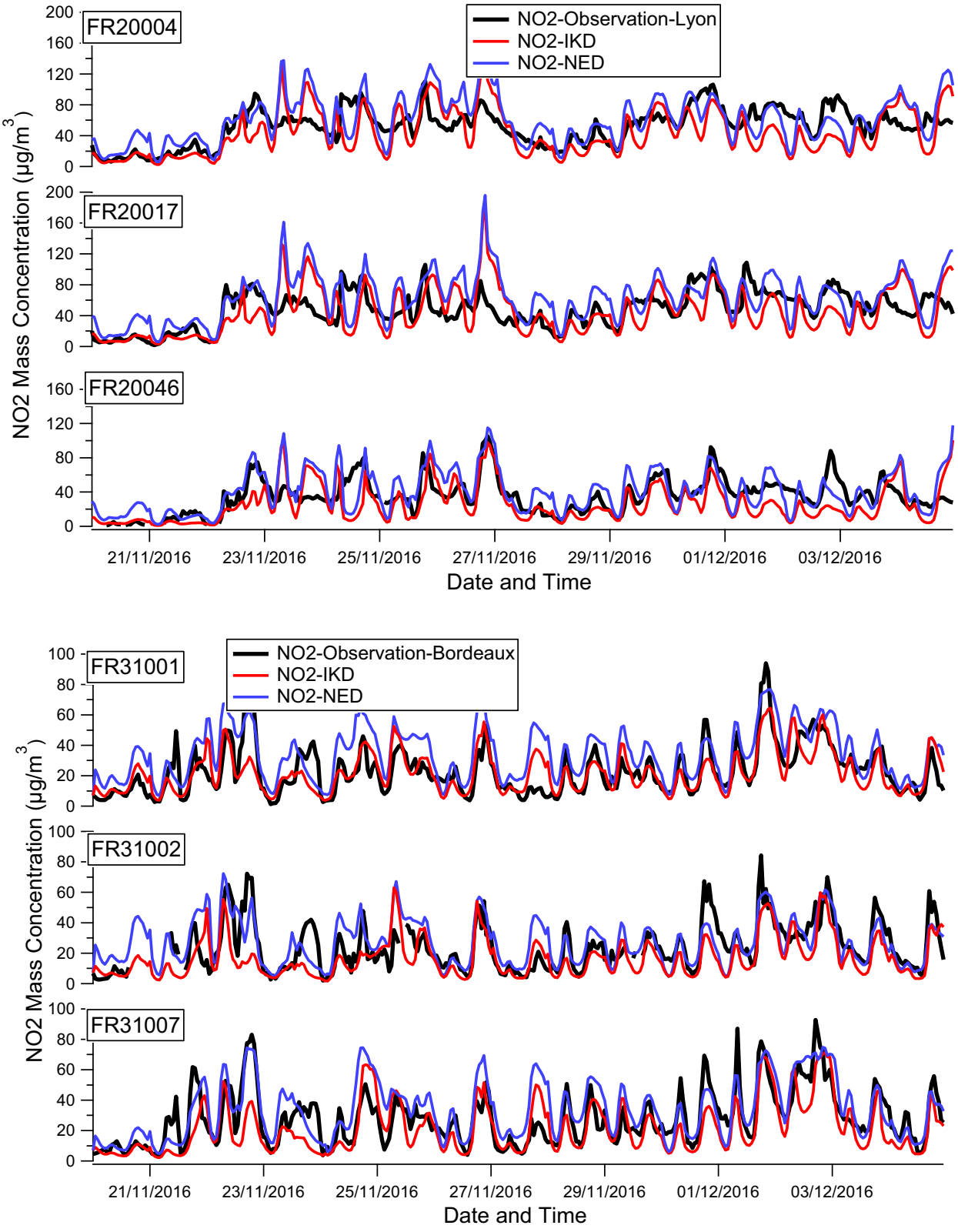

Fig. 10. Time series between observed and modeled NO_2 mass concentrations ($\mu g/m^3$) in urban background stations. FR20XXX represents the station in Lyon region and FR31XXX represents the station in Bordeaux region.

underestimates NO_2 concentrations at all urban sites especially on the period of 30th November to 3rd December. Taking the RSME as the criterion, the use of the NED scheme improves NO_2 simulation in every urban site especially in the three urban sites in the Lyon region with an average improvement of 24.51%. In general, the model has a better performance for NO_2 simulation in Bordeaux than Lyon, that because the orography of Lyon is more complex than in Bordeaux, the city is close to the Alps in a hilly region with sharp terrain gradients and the

Table 4
Average modeled NO_2 mass concentrations (Avg); the correlation (R); mean bias (MB) and root mean square error (RMSE) between Observation and simulation of NO2 in four urban background stations over Lyon and Boudreaux region.

	IKD				NED				
	Avg	R	MB	RMSE	Avg	R	MB	RMSE	improvement
FR20004	43.8	0.55	−7.8	26.9	61.1	0.60	9.4	19.2	28.3%
FR20017	44.5	0.44	−3.1	29.0	62.9	0.53	15.3	20.6	28.8%
FR20046	25.7	0.57	−12.6	20.8	40.6	0.63	2.3	17.4	16.4%
FR31001	21.9	0.71	−1.2	13.8	34.1	0.74	7.9	11.3	17.7%
FR31002	21.5	0.72	−6.3	14.3	33.5	0.77	5.1	14.3	0.01%
FR31007	16.9	0.65	−7.2	14.2	27.1	0.66	2.9	12.6	10.9%

distribution of urban land use that is more scattered than Bordeaux. The diurnal cycles for surface *Kz* and surface concentrations of NO_2 over Lyon and Bordeaux regions are provides in the Fig. S12.

3.2.5. $PM_{2.5}$ and PM_{10} simulations over Lyon and Bordeaux

The $PM_{2.5}$ and PM_{10} maps of mean concentrations in Lyon and Bordeaux domains over the period are displayed in Fig. S13 and Fig. S14, respectively. The results show the regional patterns of $PM_{2.5}$ and PM_{10} are similar for both schemes. The simulated surface $PM_{2.5}$ concentrations from NED scheme is approximately 1.6 $\mu g/m^3$ and 1.4 $\mu g/m^3$ higher on average than for the IKD scheme in Lyon and Bordeaux region respectively and gives approximately 1.6 $\mu g/m^3$ and 1.2 $\mu g/m^3$ higher PM_{10} surface concentration than IKD scheme in Lyon and Bordeaux respectively. The differences mainly occurred on the urban sites with slight differences in rural areas for both Lyon and Bordeaux domains.

The comparison of simulated $PM_{2.5}$ and PM_{10} concentrations by the IKD and NED schemes in Lyon and Bordeaux regions with observational data are presented in Fig. 11. The results show that the model could fairly capture the time variability of $PM_{2.5}$ and PM_{10} on the regular days of Lyon domain but strongly underestimates the concentrations during the PE. In Bordeaux, the model could not reproduce the $PM_{2.5}$ and PM_{10} well for the whole period, a huge underestimation occurred at all station. A previous study (Lanzafame, 2019) indicates that the biomass burning emissions are strongly underestimated in the model over the western cities of France, especially for the city of Bordeaux. The Alps region is also often affected by pollution episodes in wintertime with a large contribution of residential wood burning (Bessagnet et al., 2020). Thus, the underestimation of the biomass burning emissions over Lyon regions should be a likely explanation of the issue during the PE. The specific quantitative analysis on the model performance of PM simulation is not confirmed in this section due to large uncertainties associated to emissions mainly. The model provides satisfactory results for NO_2 simulations but cannot give a reasonable behavior of $PM_{2.5}$ and PM_{10} when compared to the observations. This indicates the issue of PM simulations in Lyon and Bordeaux regions should not due to the model configuration. Improvements on the emission inventories are required first in those regions.

4. Conclusions

The flow characteristics and dispersion mechanisms of pollutants are important for air quality simulation and forecast. In the first part of this study, three vertical diffusion coefficients based on first order local closure scheme have been compared and evaluated by a one-year simulation over France. By comparing the model performances of the three schemes in urban and rural areas, we find that the schemes perform better in rural than in urban areas. The vertical mixing is relatively overestimated in urban areas. The results also indicate such simplest scheme is an effective way to reproduce the dispersion of pollutants both in urban canopy and surroundings in mesoscale chemistry transport model, but it cannot be expected to significantly improve the mesoscale model by this simple modification based on the first-order local closure Reynolds decomposition scheme. More obvious improvements need to start with a more accurate turbulence process. This first screening of usual *K-theory* diffusion parameterizations over a long-term simulation was a first step to identify limitations and possible improvements.

The second part of the study used a 1.5-order turbulence kinetic energy-based eddy diffusivity closure scheme from WRF defined as NED on the urban air quality context to assess consequences of surface-level emission of nitrogen dioxide (NO_2) and particulate matter ($PM_{2.5}$ and PM_{10}) in Paris, Lyon and Bordeaux. The performances of the NED and initial *Kz* diffusion (IKD) scheme were evaluated by ground observations both temporally and spatially. The study in Paris indicates both schemes can capture the evolution of the NO_2, $PM_{2.5}$ and PM_{10} concentrations in urban areas even though pollutants concentrations are somewhat underestimated on the pollution episode (PE). The NED scheme shows a better ability on PE prediction and displays a better performance in urban areas for NO_2, $PM_{2.5}$ and PM_{10} simulation with an average improvement at 18.8%, 13.5% and 19.1% respectively.

The model performance in Lyon and Bordeaux confirm the results obtained in Paris. The NED scheme improves the NO_2 simulation approximately by 24.5% and 9.5% in the urban areas of Lyon and Bordeaux respectively. However, PM simulations in Lyon and Bordeaux indicate that, based on previous studies, a strong underestimation of biomass burning emissions in wintertime could be the main reason. The NED scheme gradually improves the air quality simulation in urban areas. Although the overall performance of the proposed method is better than initial model configuration, the NED scheme still slightly overestimates the concentration of major pollutants during regular day. The underestimation of *Kz* of NED is more pronounced in the nighttime than the daytime. Further improvements are necessary particularly under stable boundary conditions. In general, 1.5-order turbulence kinetic energy-based eddy diffusivity closure scheme is an effective way to improve the CTM ability particularly under stagnant conditions. It can be expected further improvement of the model ability through the use of higher-order turbulent closure schemes. The cost-benefit is also important in mesoscale modeling, the difference between the L4 and L12 cases for the operational time for simulating a single day meteorological and chemical transport processes is small, totally 149 min and 151 min, respectively. The difference in cost effectiveness between the two schemes is negligible. It is also important to notice that the results are based on a two-week simulation over early winter, longer periods are needed to further verify the reliability of the results. Meanwhile, the near-surface turbulence simulation also requires in-depth understanding and investigation, and further progress is expected in the future to have the substantial progress.

CRediT authorship contribution statement

Lei Jiang: Conceptualization, Data curation, Formal analysis, Software, Writing – original draft. **Bertrand Bessagnet:** Conceptualization, Funding acquisition, Project administration, Software, Writing – review & editing. **Frédérik Meleux:** Validation, Writing – review & editing. **Florian Couvidat:** Software, Validation, Writing – review & editing.

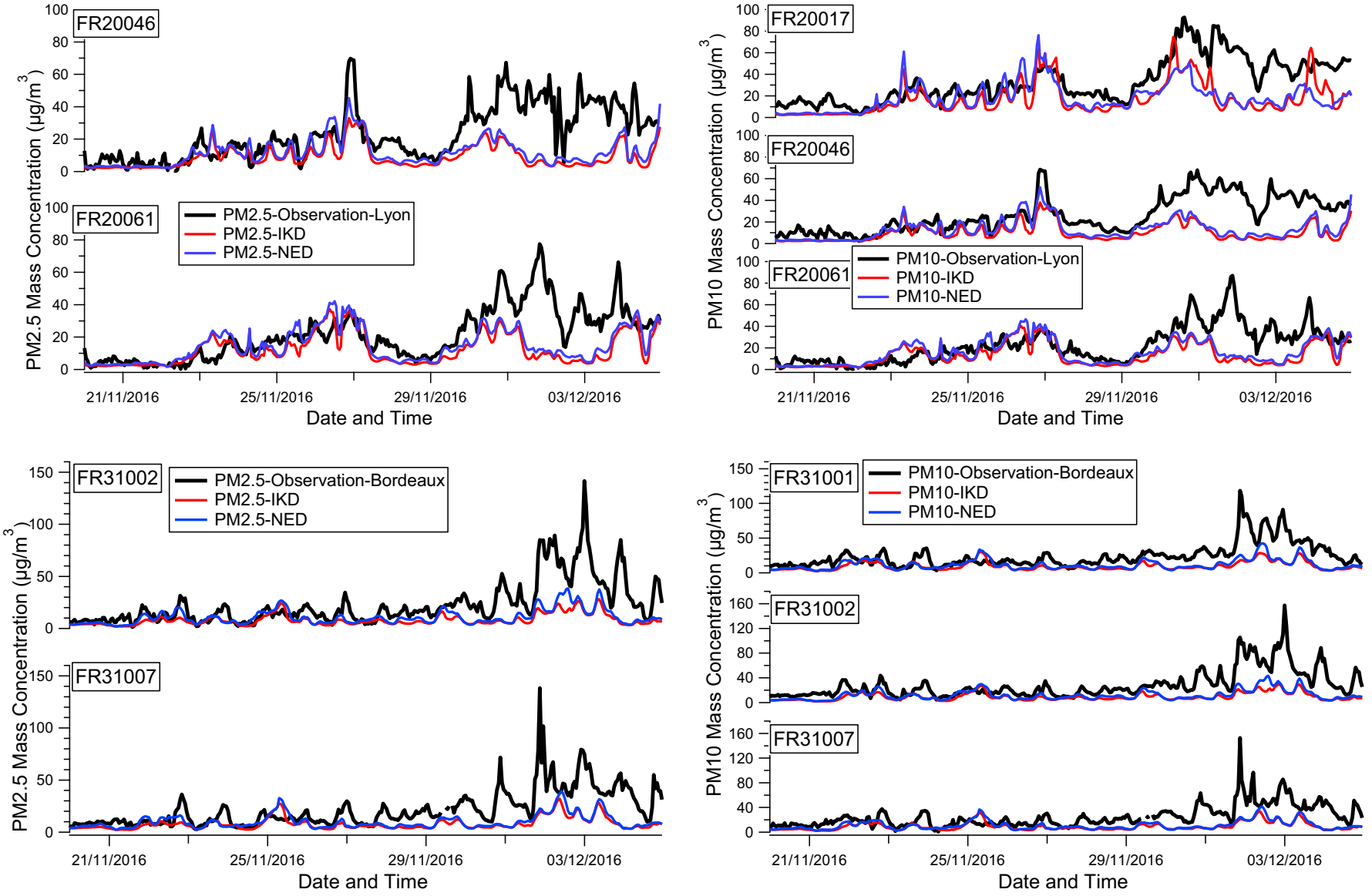

Fig. 11. Time series between observed and modeled $PM_{2.5}$ and PM_{10} mass concentrations ($\mu g/m^3$) in urban background stations. FR20XXX represents the station in Lyon region and FR31XXX represents the station in Bordeaux region.

Frédéric Tognet: Validation, Writing – review & editing.

Declaration of Competing Interest

The authors declare that they have no known competing financial interests or personal relationships that could have appeared to influence the work reported in this paper.

Data availability

Data will be made available on request.

Acknowledgements

The authors thank the French Ministry in charge of Environment (MTES) for providing funds for this research. Thanks the Météo-France for providing the planetary boundary layer height data for the Paris region to support this research. The authors acknowledge LCSQA for the use of the time-integrated ambient air quality data. The authors would like to acknowledge high-performance computing support from TGCC (http://www-hpc.cea.fr/fr/complexe/tgcc.htm) provided by the French Atomic Energy Commission (CEA).

Appendix A. Supplementary data

Supplementary data to this article can be found online at https://doi.org/10.1016/j.atmosres.2022.106394.

References

Amodio, M., Catino, S., Dambruoso, P.R., de Gennaro, G., Di Gilio, A., Giungato, P., et al., 2014. Atmospheric deposition: sampling procedures, analytical methods, and main recent findings from the scientific literature. Adv. Meteorol. 2014, 1–27. https://doi.org/10.1155/2014/161730.

Argyropoulos, C.D., Markatos, N.C., 2015. Recent advances on the numerical modelling of turbulent flows. Appl. Math. Model. 39 (2), 693–732. https://doi.org/10.1016/j.apm.2014.07.001.

Baker, J., Walker, H.L., Cai, X., 2004. A study of the dispersion and transport of reactive pollutants in and above street canyons—a large eddy simulation. Atmos. Environ. 38 (39), 6883–6892. https://doi.org/10.1016/j.atmosenv.2004.08.051.

Baklanov, A., Hänninen, O., Slørdal, L.H., Kukkonen, J., Bjergene, N., Fay, B., et al., 2007. Integrated systems for forecasting urban meteorology, air pollution and population exposure. Atmos. Chem. Phys. 7 (3), 855–874. https://doi.org/10.5194/acp-7-855-2007.

Bessagnet, B., Menut, L., Lapere, R., Couvidat, F., Jaffrezo, J.-L., Mailler, S., et al., 2020. High resolution chemistry transport modeling with the on-line CHIMERE-WRF model over the French Alps—analysis of a feedback of surface particulate matter concentrations on mountain meteorology. Atmosphere 11 (6), 565. https://doi.org/10.3390/atmos11060565.

Bougeault, P., Lacarrere, P., 1989. Parameterization of orography-induced turbulence in a mesobeta–scale model. Mon. Weather Rev. 117 (8), 1872–1890. https://doi.org/10.1175/1520-0493(1989)117<1872:POOITI>2.0.CO;2.

Byun, D., Schere, K.L., 2006. Review of the governing equations, computational algorithms, and other components of the Models-3 Community Multiscale Air Quality (CMAQ) modeling system. Appl. Mech. Rev. 59 (2), 51–77. https://doi.org/10.1115/1.2128636.

Chen, Z., Zhuang, Y., Xie, X., Chen, D., Cheng, N., Yang, L., Li, R., 2019. Understanding long-term variations of meteorological influences on ground ozone concentrations in Beijing during 2006–2016. Environ. Pollut. 245, 29–37. https://doi.org/10.1016/j.envpol.2018.10.117.

Colette, A., Granier, C., Hodnebrog, Ø., Jakobs, H., Maurizi, A., Nyiri, A., et al., 2011. Air quality trends in Europe over the past decade: a first multi-model assessment. Atmos. Chem. Phys. 11 (22), 11657–11678. https://doi.org/10.5194/acp-11-11657-2011.

Costa, A., Macedonio, G., Folch, A., 2006. A three-dimensional Eulerian model for transport and deposition of volcanic ashes. Earth Planet. Sci. Lett. 241 (3–4), 634–647. https://doi.org/10.1016/j.epsl.2005.11.019.

Deardorff, J.W., 1980. Stratocumulus-capped mixed layers derived from a three-dimensional model. Bound.-Layer Meteorol. 18 (4), 495–527. https://doi.org/10.1007/BF00119502.

Dragomir, C.M., Constantin, D.-E., Voiculescu, M., Georgescu, L.P., Merlaud, A., Roozendael, M.V., 2015. Modeling results of atmospheric dispersion of NO 2 in an urban area using METI–LIS and comparison with coincident mobile DOAS measurements. Atmos. Pollut. Res. 6 (3), 503–510. https://doi.org/10.5094/APR.2015.056.

Fillingham, M., 2019. The Influence of CMAQ Model Resolution on Predicted Air Quality and Associated Health Impacts (Master of Applied Science). Carleton University, Ottawa, Ontario. https://doi.org/10.22215/etd/2019-13420.

Folch, A., Costa, A., Macedonio, G., 2009. FALL3D: a computational model for transport and deposition of volcanic ash. Comput. Geosci. 35 (6), 1334–1342. https://doi.org/10.1016/j.cageo.2008.08.008.

Gašparac, G., Jeričević, A., Kumar, P., Grisogono, B., 2020. Regional-scale modelling for the assessment of atmospheric particulate matter concentrations at rural background locations in Europe. Atmos. Chem. Phys. 20 (11), 6395–6415. https://doi.org/10.5194/acp-20-6395-2020.

Gromke, C., Blocken, B., 2015. Influence of avenue-trees on air quality at the urban neighborhood scale. Part II: traffic pollutant concentrations at pedestrian level. Environ. Pollut. 196, 176–184. https://doi.org/10.1016/j.envpol.2014.10.015.

He, Y., McFarlane, N.A., Monahan, A.H., 2019. A new TKE-based parameterization of atmospheric turbulence in the canadian global and regional climate models. J. Adv. Model. Earth Syst. 11 (5), 1153–1188. https://doi.org/10.1029/2018MS001532.

Hirabayashi, S., Kroll, C.N., Nowak, D.J., 2012. Development of a distributed air pollutant dry deposition modeling framework. Environ. Pollut. 171, 9–17. https://doi.org/10.1016/j.envpol.2012.07.002.

Holtslag, B., Boville, B., 1993. Local versus nonlocal boundary-layer diffusion in a global climate model. J. Clim. 6, 1825–1842. https://doi.org/10.1175/1520-0442(1993)006<1825:LVNBLD>2.0.CO;2.

Honore, C., Menut, L., Bessagnet, B., Meleux, F., Rouil, L., Vautard, R., et al., 2006. PREV'AIR, a platform for air quality monitoring and forecasting. In: Presented at the AGU Fall Meeting 2006. Retrieved from. https://hal-ineris.archives-ouvertes.fr/ineris-00970155.

Hu, X.-M., Nielsen-Gammon, J.W., Zhang, F., 2010. Evaluation of three planetary boundary layer schemes in the WRF model. J. Appl. Meteorol. Climatol. 49 (9), 1831–1844. https://doi.org/10.1175/2010JAMC2432.1.

Huang, D., 2019. A new turbulence analysis method based on the mean speed and mean free path theory of the molecule thermal motion. Phys. A Stat. Mech. Appl. 523, 66–74. https://doi.org/10.1016/j.physa.2019.01.131.

Huszar, P., Karlický, J., Ďoubalová, J., Šindelářová, K., Nováková, T., Belda, M., et al., 2020. Urban canopy meteorological forcing and its impact on ozone and $PM_{2.5}$: role of vertical turbulent transport. Atmos. Chem. Phys. 20 (4), 1977–2016. https://doi.org/10.5194/acp-20-1977-2020.

Jiang, L., Bessagnet, B., Meleux, F., Tognet, F., Couvidat, F., 2020. Impact of physics parameterizations on high-resolution air quality simulations over the Paris Region. Atmosphere 11 (6), 618. https://doi.org/10.3390/atmos11060618.

Klimontovich, Yu.L., 1985. Turbulent motion. The structure of chaos. In: Haken, H. (Ed.), Complex Systems — Operational Approaches in Neurobiology, Physics, and Computers. Springer, Berlin, Heidelberg, pp. 332–341. https://doi.org/10.1007/978-3-642-70795-7_25.

Kurppa, M., Hellsten, A., Auvinen, M., Raasch, S., Vesala, T., Järvi, L., 2018. Ventilation and air quality in city blocks using Large-Eddy simulation—urban planning perspective. Atmosphere 9 (2), 65. https://doi.org/10.3390/atmos9020065.

Lanzafame, G.M., 2019, December 12. Understanding organic aerosol formation processes in atmosphere using molecular markers : a combined measurements-model approach Speciation of organic fraction does matter for source apportionment. Part 1 : A one-year campaign in Grenoble (France) Precursors and formation of secondary organic aerosols from wildfires in the Euro-Mediterranean region (These de doctorat). Sorbonne université. Retrieved from. http://www.theses.fr/2019SORUS519.

Lee, J.-H., Wu, C.-F., Hoek, G., de Hoogh, K., Beelen, R., Brunekreef, B., Chan, C.-C., 2014. Land use regression models for estimating individual NOx and NO2 exposures in a metropolis with a high density of traffic roads and population. Sci. Total Environ. 472, 1163–1171. https://doi.org/10.1016/j.scitotenv.2013.11.064.

Letzel, M.O., Krane, M., Raasch, S., 2008. High resolution urban large-eddy simulation studies from street canyon to neighbourhood scale. Atmos. Environ. 42 (38), 8770–8784. https://doi.org/10.1016/j.atmosenv.2008.08.001.

Lim, S., Kim, J., Kim, T., Lee, K., Yang, W., Jun, S., Yu, S., 2012. Personal exposures to PM2.5 and their relationships with microenvironmental concentrations. Atmos. Environ. 47, 407–412. https://doi.org/10.1016/j.atmosenv.2011.10.043.

Menut, Laurent, Bessagnet, B., Colette, A., Khvorostiyanov, D., 2013a. On the impact of the vertical resolution on chemistry-transport modelling. Atmos. Environ. 67, 370–384. https://doi.org/10.1016/j.atmosenv.2012.11.026.

Menut, L., Bessagnet, B., Khvorostyanov, D., Beekmann, M., Blond, N., Colette, A., et al., 2013b. CHIMERE 2013: a model for regional atmospheric composition modelling. Geosci. Model Dev. 6 (4), 981–1028. https://doi.org/10.5194/gmd-6-981-2013.

Novati, G., de Laroussilhe, H.L., Koumoutsakos, P., 2021. Automating turbulence modelling by multi-agent reinforcement learning. Nat. Mach. Intell. 3 (1), 87–96. https://doi.org/10.1038/s42256-020-00272-0.

Palmgren, F., Berkowicz, R., Hertel, O., Vignati, E., 1996. Effects of reduction of NOx on the NO2 levels in urban streets. Sci. Total Environ. 189–190, 409–415. https://doi.org/10.1016/0048-9697(96)05238-2.

Pierce, T., Hogrefe, C., Trivikrama Rao, S., Porter, P.S., Ku, J.-Y., 2010. Dynamic evaluation of a regional air quality model: assessing the emissions-induced weekly ozone cycle. Atmos. Environ. 44 (29), 3583–3596. https://doi.org/10.1016/j.atmosenv.2010.05.046.

Sabatier, T., Paci, A., Lac, C., Canut, G., Largeron, Y., Masson, V., 2020. Semi-idealized simulations of wintertime flows and pollutant transport in an Alpine valley: origins of local circulations (part I). Q. J. R. Meteorol. Soc. 146 (727), 807–826. https://doi.org/10.1002/qj.3727.

Simon, J.S., Zhou, B., Mirocha, J.D., Chow, F.K., 2019. Explicit filtering and reconstruction to reduce grid dependence in convective boundary layer simulations using WRF-LES. Mon. Weather Rev. 147 (5), 1805–1821. https://doi.org/10.1175/MWR-D-18-0205.1.

Sokhi, R.S., Baklanov, A., Schlünzen, K.H., 2018. Mesoscale Modelling for Meteorological and Air Pollution Applications. Anthem Press.

Stohl, A., Aamaas, B., Amann, M., Baker, L.H., Bellouin, N., Berntsen, T.K., et al., 2015. Evaluating the climate and air quality impacts of short-lived pollutants. Atmos. Chem. Phys. 15 (18), 10529–10566. https://doi.org/10.5194/acp-15-10529-2015.

Stull, R.B., 1988. Turbulence kinetic energy, stability and scaling. In: Stull, R.B. (Ed.), An Introduction to Boundary Layer Meteorology. Springer Netherlands, Dordrecht, pp. 151–195. https://doi.org/10.1007/978-94-009-3027-8_5.

Terrenoire, E., Bessagnet, B., Rouïl, L., Tognet, F., Pirovano, G., Létinois, L., et al., 2015. High-resolution air quality simulation over Europe with the chemistry transport model CHIMERE. Geosci. Model Dev. 8 (1), 21–42. https://doi.org/10.5194/gmd-8-21-2015.

Troen, I.B., Mahrt, L., 1986. A simple model of the atmospheric boundary layer; sensitivity to surface evaporation. Bound.-Layer Meteorol. 37 (1), 129–148. https://doi.org/10.1007/BF00122760.

Tyagi, B., Magliulo, V., Finardi, S., Gasbarra, D., Carlucci, P., Toscano, P., et al., 2018. Performance analysis of planetary boundary layer parameterization schemes in WRF modeling set up over Southern Italy. Atmosphere 9 (7), 272. https://doi.org/10.3390/atmos9070272.

Valari, M., Markakis, K., Powaga, E., Collignan, B., Perrussel, O., 2020. EXPLUME v1.0: a model for personal exposure to ambient O₃ and PM<sub>2.5</sub&gt. Geosci. Model Dev. 13 (3), 1075–1094. https://doi.org/10.5194/gmd-13-1075-2020.

Warner, T.T., 2010. Numerical Weather and Climate Prediction. Cambridge University Press, Cambridge. https://doi.org/10.1017/CBO9780511763243.

Wise, D.K.A.G., 2016. ICIE 2016 Proceedings of the 4th International Conference on Innovation and Entrepreneurship: ICIE2016. Academic Conferences and publishing limited.

Wolf, T., Pettersson, L.H., Esau, I., 2020. A very high-resolution assessment and modelling of urban air quality. Atmos. Chem. Phys. 20 (2), 625–647. https://doi.org/10.5194/acp-20-625-2020.

Wolf-Grosse, T., Esau, I., Reuder, J., 2017. Sensitivity of local air quality to the interplay between small- and large-scale circulations: a large-eddy simulation study. Atmos. Chem. Phys. 17 (11), 7261–7276. https://doi.org/10.5194/acp-17-7261-2017.

Wyngaard, J.C., 2004. Toward numerical modeling in the "Terra Incognita.". J. Atmos. Sci. 61 (14), 1816–1826. https://doi.org/10.1175/1520-0469(2004)061<1816:TNMITT>2.0.CO;2.

Zilitinkevich, S.S., Esau, I.N., 2005. Resistance and heat-transfer laws for stable and neutral planetary boundary layers: old theory advanced and re-evaluated. Q. J. R. Meteorol. Soc. 131 (609), 1863–1892. https://doi.org/10.1256/qj.04.143.